

Airy beams from a microchip laser

Stefano Longhi

Dipartimento di Fisica, Politecnico di Milano, Piazza L. da Vinci 32, I-20133 Milano, Italy

Compiled March 9, 2021

It is theoretically shown that an end-pumped microchip laser formed by a thin laser crystal with plane-plane but slightly tilted facets can emit, under appropriate pumping conditions and near a crystal edge, a truncated self-accelerating Airy output beam. © 2021 Optical Society of America

OCIS codes: 140.3410, 350.5500, 190.4420, 140.3580

Microchip lasers are an important class of monolithic solid-state lasers which have attracted a considerable interest as single-frequency and ultracompact devices [1–3]. A microchip laser generally consists of a thin rare-earth-doped laser crystal with dielectric coatings on both faces to form a plane parallel cavity, end-pumped by a diode laser. Owing to the planar nature of the cavity, the transverse modes of a microchip laser are not determined by mirror curvatures, rather by weaker, residual guiding effects, such as gain or thermally-induced guiding [4–9]. In this Letter we consider a microchip laser with two planar but slightly tilted facets, and show that end-pumping near the edge of the laser crystal can lead to laser emission into self-accelerating Airy beams, a class of optical beams which has received a great interest in the recent few years [10–17]. Airy beams show rather unique properties, such as diffraction free propagation along a curved (parabolic) path and self healing, i.e., restoring their canonical form after passing small obstacles. Airy beams found recently important applications in optics, including optical trapping [12], plasma waveguiding [15] and nonlinear frequency generation [16, 17].

Let us consider a microchip laser operating at the wavelength λ made of a thin crystal (length l , refractive index n_s) with two highly-reflecting and dielectric-coated planar facets [Fig.1(a)]. For the sake of simplicity, we first consider the case of a one transverse spatial coordinate. The two crystal facets are not perfectly parallel each other, but are tilted to form a small angle α_x . The microchip is end-pumped by a Gaussian beam, focused at a distance ρ_x from the upper edge of the crystal [see Fig.1(a)]. Field propagation in the cavity can be described within an effective-index and mean-field model [9], in which the intracavity field envelope ψ is assumed to slightly vary in one cavity round trip. Propagation back and forth between the two mirrors is equivalent to propagation along a lensguide with a complex refractive index $n(x) = n_s + \Delta n(x) \simeq n_s$, where the real and imaginary parts of $\Delta n(x)$ account for (weak) index and gain guiding effects, respectively [9]. Let $\psi(x)$ be the field envelope at the reference plane $z = 0$ in the cavity; after a cavity round-trip, the field envelope is transformed into the one $\psi'(x) = \hat{T}\psi(x)$, where \hat{T} is the

round-trip propagation operator given by

$$\hat{T} = \exp(-\gamma) \exp(-ikl\hat{H}) \exp(-ikn_s\alpha_x x) \exp(-ikl\hat{H}). \quad (1)$$

In Eq.(1), $k = 2\pi/\lambda$ is the wave number, γ is the single-pass logarithmic loss of the cavity [18], and

$$\hat{H} = -1/(2n_s k^2) \partial_x^2 - \Delta n(x). \quad (2)$$

Note that $\psi'(x)$ is obtained from $\psi(x)$ by application of the four operators $\hat{T}_1 = \exp(-\gamma)$, $\hat{T}_2 = \exp(-ikl\hat{H})$, $\hat{T}_3 = \exp(-ikn_s\alpha_x x)$ and $\hat{T}_4 = \hat{T}_2$ describing the effects of cavity loss, forward propagation in the crystal, phase shift introduced by the mirror tilt, and backward propagation in the crystal, respectively. In the mean-field limit, one can assume $\hat{T} \simeq 1 - \gamma - 2ikl\hat{H} - ikn_s\alpha_x x$. Indicating by $T_R = 2ln_s/c_0$ the round-trip transit time in the cavity, where c_0 is the speed of light in vacuum, the temporal evolution of the field envelope $\psi(x, t)$ is then given by $\partial_t \psi(x, t) \simeq [\psi'(x) - \psi(x)]/T_R$, i.e.

$$\partial_t \psi = -\frac{\psi}{2\tau_c} + i\frac{c_0}{2n_s^2 k} \partial_x^2 \psi + ikc_0 \left(\frac{\Delta n}{n_s} - \frac{\alpha_x x}{2l} \right) \psi, \quad (3)$$

where $\tau_c = T_R/(2\gamma)$ is the cavity photon lifetime. Neglecting thermal lensing effects [7] and assuming that the laser operates at the resonance frequency of the gain medium, so that gain-related index guiding effects can be neglected as well [7, 9], the refractive index Δn in Eq.(3) can be taken to be purely imaginary and given by $\Delta n(x) = -i\sigma_g N(x)/(2k)$, where σ_g is the cross-section of the lasing transition and $N(x)$ is the (saturated) population inversion distribution in the crystal. For a Gaussian pump beam with a Rayleigh range larger than the crystal thickness l and for the laser operated near threshold, for which saturation effects can be neglected [7], one has $N(x) = N_0(x) = N_p \exp[-2(x - \rho_x)^2/w_p^2]$, where w_p is the pump beam spot size. Above threshold, in the mean-field limit and neglecting spatial hole burning, following Ref. [8] saturation effects can be included in the model by taking $N(x) = N_0(x)/(1 + |\psi|^2)$, where the intracavity field intensity is normalized to the saturation intensity of the lasing transition. The on-axis single-pass (unsaturated) photon gain coefficient g_p in the medium is related to the (unsaturated) peak population inversion N_p by the simple relation $g_p = \sigma_g N_p l$ [18]. Crystal truncation at $x = 0$ introduces an effective barrier potential

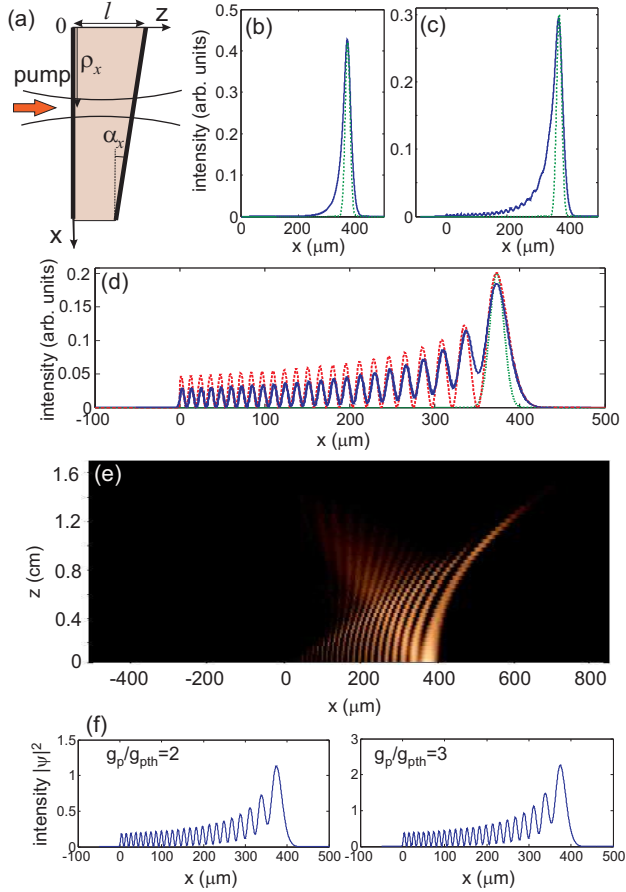


Fig. 1. (Color online) (a) Schematic of an end-pumped microchip laser with tilted mirror. (b)-(d) Numerically-computed transverse mode profile at lasing threshold (solid curve) for decreasing values of the logarithmic cavity loss, showing the transition from an asymmetric Gaussian beam to a truncated Airy beam: (b) $\gamma = 0.142$, (c) $\gamma = 0.0651$, and (d) $\gamma = 0.019$. The gain threshold $g_p = g_{pth}$ is $g_{pth} = 0.326$ in (b), $g_{pth} = 0.2172$ in (c), and $g_{pth} = 0.1086$ in (d). The dotted curve in the figures is the profile of the Gaussian population inversion ΔN_0 , whereas the dashed curve in (d) is the intensity profile of the Airy mode $|\psi_n|^2$ with $\xi_n = 23.224$. (e) Free-space propagation of the output laser beam of Fig.1(d) [intensity distribution in the (x, z) plane]. (f) Same as (d), but for a gain parameter g_p two times (left panel) and three times (right panel) above threshold.

for the paraxial lasing field because of total internal reflection, which is modeled by requiring $\psi = 0$ for $x \leq 0$ in Eq.(3). As discussed below, such an edge effect is of major importance for the laser to oscillate on a (truncated) Airy transverse mode. Introducing the normalized spatial and temporal variables $\xi = x/L$ and $\tau = t/T$, where

$$L = \left(\frac{l}{n_s^2 \alpha_x k^2} \right)^{1/3}, \quad T = \frac{2}{c_0} \left(\frac{l^2 n_s^2}{\alpha_x^2 k} \right)^{1/3}, \quad (4)$$

Eq.(3) can be cast in the dimensionless form

$$\partial_\tau \psi = i \partial_\xi^2 \psi - i \xi \psi + \frac{T}{T_R} \left(\frac{g_p F}{1 + |\psi|^2} - \gamma \right) \psi \equiv \hat{Q} \psi, \quad (5)$$

where $F = F(\xi) = \exp[-2(\xi L - \rho_x)^2/w_p^2]$ is the normalized profile of the unsaturated population inversion in the crystal and $g_p = \sigma_g N_p l$ the peak gain coefficient. The thresholds and profiles of the various transverse modes sustained by the microchip laser can be computed by numerical analysis of eigenvalues and eigenfunctions of the (linear) operator \hat{T} by taking $\Delta N(x) = \Delta N_0(x)$. In particular, the lowest-order lasing mode can be computed by a standard Fox-Li iterative method [19]. The profile of the lasing mode turns out to depend mainly on the two parameters $(T/T_R)\gamma$ and ρ_x/L , i.e. by the logarithmic cavity loss, tilting angle, and distance of the pump beam from the crystal edge. This is because two different physical mechanisms compete in the formation of the transverse laser mode. On the one hand, gain guiding provided by the pump tends to localize the lasing mode near the gain region, as in usual microchip lasers with parallel facets [4–8]; on the other hand, the mirror tilting pushes the light beam toward the edge of the crystal, where it is back reflected owing to total internal reflection, thus providing an effective trapping of light which was discussed in [20] in another optical setting. Depending on the strength of these two competing processes, two distinct transverse confining regimes can be found. When ρ_x/L_x is very large (i.e. the crystal is pumped far from the crystal edge) and the cavity losses are not too small (i.e. the gain guide is strong enough), the gain-guiding mechanism prevails and the lasing mode looks like a slightly asymmetric Gaussian beam, similar to the off-axis Gaussian modes with complex arguments studied in [21, 22]. Conversely, if the crystal is pumped closer to the edge of the crystal and the logarithmic cavity loss γ is sufficiently small, the edge trapping mechanism prevails. In this case, gain and loss terms entering on the right hand side of Eq.(5) can be treated as perturbation terms, and the transverse mode profiles of the cold cavity are defined by the Airy equation $\partial_\xi^2 \psi - \xi \psi = \sigma \psi$ with the boundary condition $\psi(0) = 0$, i.e. $\psi_n(\xi) = \text{Ai}(\xi + \xi_n)$, where ξ_n is the n th zero of the Airy function and $\sigma = \xi_n$ is the eigenvalue that determines the transverse mode frequency. Hence, the lasing mode will be determined by the (truncated) Airy eigenmode $\psi_n(\xi)$ with the largest overlap with the pump beam profile. As an example, Figs.1(b-d) show the transition of the lasing mode at threshold from an asymmetric Gaussian-like beam to a truncated Airy beam. In the simulations, different crystals were considered, with decreasing values of cavity loss γ (controlled e.g. by the mirror reflectance) and equal distance ρ_x of the pump beam from the crystal edge. The lowest-order (lasing) mode at threshold has been computed by the Fox-Li iterative method using the exact round-trip propagator \hat{T} , defined by Eq.(1). Parameter values used in the numerical simulations refer to

a Nd:YVO₄ microchip laser [7, 8] ($n_s = 2.17$, $\lambda = 1064$ nm) with crystal thickness $l = 400$ μm and tilt angle $\alpha_x = 0.5$ mrad, which correspond to spatial and temporal scales $L \simeq 17$ μm and $T \simeq 53$ ps [see Eq.(4)]. The pump distance from the crystal edge is $\rho_x = 373$ μm , whereas the pump spot size is $w_p = 17$ μm . As for large cavity losses the gain guiding is the dominant mechanism of transverse confinement and the lasing mode looks like a slightly asymmetric Gaussian beam [Fig.1(b)], at lower cavity losses index guiding provided by edge reflection and mirror tilt prevails and the lasing mode is well approximated by a truncated Airy beam with its largest lobe overlapped with the pump beam [see Fig.1(d)]. The free-space propagation of the output beam in this case is depicted in Fig.1(e), clearly showing the characteristic parabolic (accelerated) path of the Airy beams. It should be noted that the transition from Gaussian-like to Airy-like modes shown in Fig.1 could be observed by assuming different microchip lasers with equal loss γ but with increasing tilt angle α_x . Laser emission in the Airy-like mode persists for the microchip operated well above threshold, where saturation effects can not be neglected. As an example, Fig.1(f) shows the numerically-computed steady-state lasing modes, which account for saturation of the population inversion, for the same conditions of Fig.1(d) but for the laser operated with a gain parameter g_p two and three times above threshold. As one can see, gain saturation does not appreciably modify the transverse mode profile.

The previous analysis can be extended to the case of

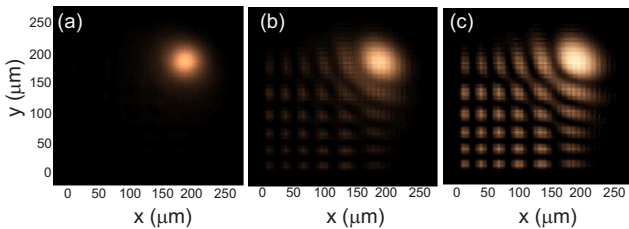


Fig. 2. (Color online) Two-dimensional transverse intensity profile $|\psi(x, y)|^2$ of the lasing mode at threshold for (a) $\gamma = 0.0632$, (b) $\gamma = 0.0298$, and (c) $\gamma = 0.0106$ (other parameter values are given in the text). The gain threshold is $g_{pth} = 0.354$ in (a), $g_{pth} = 0.236$ in (b), and $g_{pth} = 0.118$ in (c).

two-transverse spatial variables x and y . Indicating by α_x and α_y the mirror tilting angles with respect to the x and y axes, in terms of the dimensionless variables $\xi = x/L_x$, $\eta = y/L$ and $\tau = t/T$, where L and T are defined by Eq.(4), the evolution equation of the field envelope ψ in the mean-field limit reads $\partial_\tau \psi = \hat{Q} \psi$, where $\hat{Q} = i[\partial_\xi^2 + \partial_\eta^2 - \xi - (\alpha_y/\alpha_x)\eta] + (T/T_R)[g_p F/(1 + |\psi|^2) - \gamma]$, and $F = F(\xi, \eta)$ is the normalized profile of the population inversion in the crystal. For a circular Gaussian pump beam with spot size w_p focused at the point (ρ_x, ρ_y) in the transverse plane, one has $F(\xi, \eta) = \exp[-2(\xi L - \rho_x)^2/w_p^2 - 2(\eta L - \rho_y)^2/w_p^2]$.

Provided that the gain guiding is weaker than the index guiding realized by the mirror tilt and reflection at the edges, the output laser mode is expected to be given by a two-dimensional truncated Airy beam, with its main lobe mostly overlapped with the Gaussian pump beam. As an example, Fig.2 shows the numerically-computed two-dimensional distributions of the most unstable laser mode in a Nd:YVO₄ microchip laser, with a transition from a Gaussian-like to a two-dimensional truncated Airy profiles, for decreasing values of the logarithmic cavity losses γ and for $l = 400$ μm , $\alpha_x = \alpha_y = 0.2$ mrad, $\rho_x = \rho_y = 184$ μm , $w_p = 23$ μm .

In conclusion, it has been shown that microchip lasers with slightly tilted facets can emit transverse output beams in the form of truncated Airy beams. Such a result could be of interest for a direct generation of Airy beams from an ultracompact microchip device.

Work supported by the italian MIUR (Grant No. PRIN-2008-YCAAK).

References

1. J.J. Zayhowski and A. Mooradian, *Opt. Lett.* **14**, 24 (1990)
2. J.J. Zayhowski, *Laser Focus World* **35**, 129 (1999).
3. P. Laporta, S. Taccheo, S. Longhi, O. Svelto, and G. Sacchi, *Opt. Lett.* **18**, 1232 (1993).
4. G. K. Harkness and W. J. Firth, *J. Mod. Opt.* **39**, 2023 (1992).
5. T. Y. Fan, *Opt. Lett.* **19**, 554 (1994).
6. S. Longhi, *J. Opt. Soc. Am. B* **11**, 1098 (1994).
7. S. Longhi, G. Cerullo, S. Taccheo, V. Magni, and P. Laporta, *Appl. Phys. Lett.* **65**, 3042 (1994).
8. A.J. Kemp, R.S. Conroy, G.J. Friel, and B.D. Sinclair, *IEEE J. Quant. Electron.* **35**, 675 (1999).
9. C. Serrat, M.P. van Exter, N.J. van Druten, and J.P. Woerdman, *IEEE J. Quant. Electron.* **35**, 1314 (1999).
10. G.A. Siviloglou, and D. N. Christodoulides, *Opt. Lett.* **32**, 979 (2007).
11. G.A. Siviloglou, J. Brokly, A. Dogariu, and D.N. Christodoulides, *Phys. Rev. Lett.* **99**, 213901 (2007).
12. M. Mazilu, K. Dholakia, and J. Baumgart, *Nature Photon.* **2**, 675 (2008).
13. M.A. Bandres, *Opt. Lett.* **33**, 1678 (2008).
14. J. Broky, G.A. Siviloglou, A. Dogariu, and D.N. Christodoulides, *Opt. Express* **16**, 12880 (2008).
15. P. Polynkin, M. Kolesik, J.V. Moloney, G.A. Siviloglou, and D.N. Christodoulides, *Science* **324**, 229 (2009).
16. T. Ellenbogen, N. Voloch-Bloch, A. Ganany-Padowicz, and A. Arie, *Nature Photon.* **3**, 395 (2009).
17. I. Dolev, T. Ellenbogen, and A. Arie, *Opt. Lett.* **35**, 1581 (2010).
18. O. Svelto, *Principles of Lasers* (Fourth Edition, Springer, 1998).
19. A. O. Fox and T. Li, *Bell Syst. Tech. J.* **40**, 453 (1961).
20. G. Della Valle, M. Savoini, M. Ornigotti, P. Laporta, V. Foglietti, M. Finazzi, L. Duo, and S. Longhi, *Phys. Rev. Lett.* **102**, 180402 (2009).
21. L.W. Casperson, *J. Opt. Soc. Am.* **66**, 1373 (1976).
22. S. Longhi, *Opt. Lett.* **25**, 811 (2000)].